Transient Electric Birefringence Study of the Persistence Length and Electrical Polarizability of Restriction Fragments of DNA

John G. Elias and Don Eden*

Sterling Chemistry Laboratory, Yale University, New Haven, Connecticut 06511.
Received July 11, 1980

ABSTRACT: The transient electric birefringence of DNA restriction fragments ranging from 64 to 5000 base pairs and nearly monodisperse deproteinized 145 base pair nucleosomal DNA has been studied as a function of counterion concentration and degree of polymerization. Refined experimental techniques with a birefringence sensitivity of 4×10^{-12} permitted measurements to be made on very dilute solutions at low electric fields. The electrical polarizability was found to increase with the cube of the contour length for fragments less than 120 base pairs and to reach a limiting linear length dependence after 267 base pairs. This length dependence agrees with the predictions of the Mandel polarizability theory for cylindrical rods if the contour length is replaced by the average projection along the DNA's major axis. The polarizability of NaDNA and MgDNA was found to decrease linearly with the log of the counterion concentration between 0.5 and 10 mM salt, in qualitative agreement with Fixman's recent theory. It is shown from the field-free rotational diffusion measurements that DNA in 1 mM Na^+ solution begins to depart from strictly rigid rod behavior after approximately 120 base pairs and that the persistence length determined from Hearst's weakly bending rod model is 500 Å.

There has been an increasing interest recently in the electric birefringence and electric dichroism of rodlike DNA,[1,2] which has been stimulated primarily by the desire to understand the hydrodynamics, the flexibility, and the electrical polarizability characteristic of these low molecular weight polyions.

DNA can be used as the prototypical polyelectrolyte system for the study of hydrodynamic interactions as well as electrooptic properties, since many aspects of its physical and chemical structure have been well characterized. It is presently possible to make electrooptic measurements on dilute samples of monodisperse sequenced DNA restriction fragments using signal averaging techniques and low applied electric fields for which the average orientation of the polyelectrolyte is extremely small.

The electrooptical methods of transient electric birefringence and electric dichroism are the most sensitive means for determining the polarizability and the hydrodynamic behavior of polyelectrolytes in low (<100 mM) ionic strength solutions. In each of these methods the molecules in solution are partially oriented by a pulsed electric field, and the buildup and decay of the orientation process are followed optically. For rodlike molecules the orientation time depends very nearly on the cube of the length and therefore deviations from rodlike behavior are easily detected. The amplitude of the electrooptic signal is a function of the electric field strength and the polarizability of the polyion. In general, polyelectrolytes exhibit an extremely large polarizability which is attributed to polarization of the polyion's counterion atmosphere.

Hogan et al.[1] have recently studied the high-field electric dichroism of short DNA in which two restriction fragments (160 and 230 base pairs) were used along with fractionated calf thymus DNA to determine the hydrodynamic and electrical properties. A sedimentation velocity study by Kovacic and van Holde[3] has been reported in which DNA restriction fragments spanning a large molecular weight range were used to characterize the hydrodynamic properties of rigid and flexible DNA in terms of a persistence length.

For this study, we used the technique of high-sensitivity electric birefringence to measure the rotational diffusion constants and the electrical polarizabilities of a series of DNA restriction fragments that range from 64 to 5000 base pairs and of nearly monodisperse 145 base pair nucleosomal DNA.

In the theoretical section that follows, we review briefly the existing theories for the rotational diffusion constant of a straight cylinder,[4-6] a wormlike coil, and a weakly bending rod.[7] We also discuss the theoretical models that are available which describe the polarizability of rigid rod polyelectrolytes.[8-13]

Theory

Rotational Diffusion Constant. The rotational relaxation times depend on the hydrodynamic properties of a macromolecule through its rotational diffusion tensor, which for dilute solutions is determined by the molecule's shape. For DNA that is not long enough to be considered a Gaussian coil the shape can be described by wormlike or by weakly bending rod models which are characterized by a chain rigidity parameter (the persistence length), by the distance between frictional elements along the chain, and by the diameter of each element.[7] The persistence length is a measure of how far a flexible macromolecule persists in one direction along the chain, and it is equal to half the Kuhn statistical length, λ^{-1}.

Very short DNA is rigid enough to be modeled by a right circular cylinder, which is described only by its length and diameter. Because its application to experiment is simpler, there has been a tendency in the past to apply the rigid rod model to systems where the use of nonrodlike models would have been more accurate. The earlier studies on DNA used the rigid rod approximation because the molecular weight region where DNA behaves like a straight cylinder was not known and the nonrodlike models required too many parameters. In order to determine the persistence length from the rotational diffusion constants the relaxation times must be accurately measured for a series of monodisperse samples spanning a large range of molecular lengths and must be compared to the results predicted by the nonrodlike theories. Recently, sequenced restriction fragments of DNA have become available, and it is now possible to undertake these experiments.

In general, the rotational diffusion constant of right circular cylinders is given by[4]

$$D_r = \frac{3kT}{\eta_0 \pi L^3}(\ln (L/d) - \gamma_r) \qquad (1)$$

where η_0 is the solvent viscosity, kT is the thermal energy, L is the rod length, d is the rod diameter, and γ_r is a frictional factor which depends on the exact model.[5,6] Broersma[5] considered specific end effects and determined

0024-9297/81/2214-0410$01.25/0

γ_r for long cylinders. His result was

$$\gamma_r = 0.877 - 7\left(\frac{1}{\ln (2L/d)} - 0.28\right)^2 \quad (2)$$

More recently Yoshizaki and Yamakawa[6] have constructed an expression for D_r from numerical solutions using classical hydrodynamics, which takes into account the end effects, and therefore is valid for very short cylinders. Their results for the rotational diffusion constant closely approach the values calculated with Broersma's equation when the axial ratio is large, i.e., $L/d > 60$. For DNA, an axial ratio of 60 corresponds to a rather long molecule, and it is doubtful that it is rigid enough under any salt conditions to be modeled by a straight cylinder. For low axial ratios the two theories differ by as much as 30% in the predicted values of D_r. Yoshizaki and Yamakawa's empirical interpolation formula for γ_r depends on the type of spheroid cylinder under consideration. If the macromolecule has spherical ends

$$\gamma_r = 0.447 + 8.26[\ln (1 + (L/d))]^{-1} - \sum_{j=1}^{6} a_j (L/d)^{-j/4} \quad (3)$$

where the a_j's have been tabulated in their paper.

Hearst[7] derived equations for the rotational diffusion constants of wormlike and weakly bending rod molecules by using the methods developed by Riseman and Kirkwood[14] and Hermans and Ullman[15] for cases where excluded-volume effects are negligible. His treatment considered only the rotation of the entire molecule in which changes in internal coordinates were not allowed. The resulting form of the rotational diffusion constant for a wormlike coil about its minor axis is

$$D_r = \frac{kT\lambda}{\eta_0 L^2}[0.506(2\lambda L)^{1/2} - 0.636 \ln (b\lambda) - 1.548 + 0.64(b/a)] \quad (4)$$

where b is the distance between frictional elements, a is the Stokes diameter of each element, and L is the contour length of the wormlike coil. For short contour lengths the wormlike coil is less flexible and can be considered to be a weakly bending rod. Hearst's expression for the rotational diffusion constant of the weakly bending rod, which was derived by assuming that $\lambda L/2 \ll 1$, is

$$D_r = \frac{kT}{\eta_0 \pi L^3}[3 \ln (L/b) - 7.0 + 4(b/a) + \lambda L(2.25 \ln(L/b) - 6.66 + 2(b/a))] \quad (5)$$

Ionic Polarizability. The electric field orientation of polyelectrolytes such as DNA is thought to occur because the counterions surrounding the polyion are polarized by the field. The resulting dipole, which is mainly parallel to the long axis of the polyelectrolyte, is forced to align in the electric field. Orientation ceases when the thermal disorienting forces equal the electric orienting forces. Nearly complete alignment of the molecules can occur at very large electric fields.

There have been many theoretical treatments in the past 20 years that have attempted to describe the length and counterion dependence of the ionic polarizability for rodlike polyions. Mandel[8] used a model that emphasized the discrete distribution of polyion charges to derive the polarizability and the relaxation time of polarization of cylindrical, highly charged polyions due to the longitudinal motion of bound counterions. The bound counterions were constrained to a region close to the polyion where the electrostatic potential was greater than kT. Potential energy minima were located at the charged sites attached to the polyion, and the dipole moment induced by an external electric field was calculated from the probability of locating counterions a certain distance away from their minimum energy positions. The polarizability, $\Delta\alpha$, was given by

$$\Delta\alpha = \gamma z e_0^2 N L^2/12kT \quad (6)$$

where L is the length of the rod, N is the number of charged sites, γ is the fraction of bound counterions, e_0 is the elementary electric charge, and z is the valence of the counterions. Since his treatment neglected counterion–counterion repulsion, it showed that the polarizability would increase with increasing fraction of bound counterions. Equation 6 also indicates that the polarizability depends on the length cubed of the straight cylindrical polyion.

Oosawa[9] treated the polarizability by expanding the fluctuation of the counterion distribution in a Fourier series in order to get the mean-square dipole moment due to the concentration fluctuation of counterions along the polyion. The polarizability was calculated from the mean-square dipole moment, $\langle\mu^2\rangle$, according to

$$\Delta\alpha = \left.\frac{\langle\mu^2\rangle}{kT}\right|_{E\to 0} = \frac{\gamma z e_0^2 N L^2}{2\pi^2 kT}\sum_j \frac{1}{j^2}\left(\frac{1}{1 + \gamma N \phi_j/2kT}\right) \quad (7)$$

The resulting expression is similar to Mandel's result but includes a counterion interaction term, ϕ_j, which acts to alter the polarizability due to the strong interaction forces between the counterions.

It was pointed out by Oosawa[9] that in the case of sufficiently long rods ϕ_j is independent of j for small values of j. Moreover, if a long cylindrical free volume model is used, ϕ_j may be replaced by $2 \ln (R_v/a)$, where R_v is the radius of the cylindrical free volume for a single polyion and a is the radius of the cylindrical counterion phase around the polyions. It was shown by Hornick and Weill[10] that this substitution predicted the correct trend for the magnitude of the polarizability as a function of counterion concentration, provided that the parameter a varied inversely with the concentration. This approach, however, requires an independent estimation of the radius of the counterion phase. Equation 7 under these conditions becomes

$$\Delta\alpha = \frac{\gamma z e_0^2 N L^2}{12kT}\left(\frac{1}{1 + A \ln (R/a)}\right) \quad (8)$$

with $A = 2z^2\gamma e_0^2/DkT(\mathrm{RPB})$, D is the dielectric constant, and RPB is the charge spacing.

Warashina and Minakata[11] were able to treat the problem of counterion polarization by using a discrete site model based on Oosawa's formulation. The Fourier transform of the counterion interaction potential, ϕ_j, obtained by this approach is easily evaluated for cases where the interaction is assumed to be Coulombic or screened Coulombic.

Manning[12] treated the ionic polarization problem in terms of a charge density parameter and the Debye–Hückel screening parameter. His result is also similar to Mandel's expression and thus gives the same length dependence, but it differs in that the fraction of bound counterions is determined theoretically and it has an explicit ionic strength dependence. The polarizability as given by Manning's theory is

$$\Delta\alpha = \frac{\gamma z e_0^2 N L^2}{12kT}\left(\frac{1}{1 - [2\gamma/(1-\gamma)] \ln (L/N\kappa^{-1})}\right) \quad (9)$$

where κ^{-1} is the Debye length, $\gamma = (1 - |z|^{-1}\xi^{-1})$, and $|z|^{-1}\xi^{-1}$ is the charge fraction. The polarizability is shown to increase with increasing counterion concentration.

A more recent theory on the polarizability of rodlike polyions has been given by Fixman,[13] who has used a different approach to the problem. Fixman starts with the Smoluchowski equation of motion for the singlet densities of small ions and used the mean-field approximation for the electrical forces. His model of the polyion is a smooth impenetrable dielectric cylinder charged to a uniform surface density. He considers the charge flux into the double layer surrounding the polyion and shows that it is significant, whereas the previously mentioned theories ignore the flux of small ions. At finite salt concentrations a leakage of counterions through the double layer reduces the induced dipole moment. He has based the calculation of the counterion flux on a boundary value approach which is strictly valid only for thin double layers. However, he gives arguments to justify the qualitative applicability of this theory at low salt concentration.

The dipole moment, μ, induced by an external electric field is given by

$$\mu = \int_{-L/2}^{L/2} ZV(Z)\, dZ \tag{10}$$

where Z is the coordinate along the major axis and $V(Z)$ is the perturbation in solution charge per unit length. $V(Z)$ is related to the electrostatic potential along the long axis, which itself obeys an integral equation similar to that for a conducting rod in an insulating fluid. For cases where the equilibrium number of counterions per unit length of cylinder, ϵ, is not very large, $V(Z)$ can be approximated by

$$V(Z) = \frac{KDq_1E_0}{q_1 - q_2} \frac{\sinh(\rho z)}{\rho \cosh(\rho L/2)} \tag{11}$$

where q_1 and q_2 are, respectively, the counterion and coion charges, E_0 is the steady-state electric field, assumed here to be equal to the applied field, D is the dielectric constant, and K and ρ are given by

$$K = [2 \ln(4L/d) - 14/3]^{-1} \tag{12}$$

$$\rho = (4\pi\bar{c}_1K/\epsilon)^{1/2} \tag{13}$$

where $\bar{c}_1$ is the counterion concentration.

Substitution of eq 11 in eq 10 gives the polarizability

$$\Delta\alpha = \frac{q_1KDL}{(q_1 - q_2)\rho^2}\left[1 - \frac{\tanh(\rho L/2)}{\rho L/2}\right] \tag{14}$$

where the polarizability perpendicular to the cylinder is assumed to be small in comparison to the parallel component.

Equation 14 predicts that the polarizability will vary linearly with the length squared of the rodlike polyion. This is in contrast to previous theories which predict a cubic length dependence, with the exception of the work by McTague and Gibbs[16] that suggests a linear dependence at low degrees of polymerization ($<10^3$) and a quadratic dependence for higher values. The polarizability is also seen from eq 14 to decrease with increasing counterion concentration.

Electric Birefringence. When appropriately oriented linearly polarized light passes through a dilute solution of ordered optically anisotropic molecules, one of the components of the light is retarded. The amount of retardation depends on the degree of ordering and on the magnitude of the intrinsic optical anisotropy of each molecule. The time dependence of the retardation, δ, is given by

$$\delta(t) = \frac{2\pi l}{\lambda_0}\Delta n_s\phi(\mu,\alpha,t) \tag{15}$$

where Δn_s is the difference in the parallel and perpendicular indices of refraction for a completely ordered system, l is the effective distance the light travels through the sample, λ_0 is the wavelength of the incident light in a vacuum, and $\phi(\mu,\alpha,t)$ is the orientational function which ranges from 0 to 1, with μ the permanent dipole moment and α the polarizability.

Various methods have been used to obtain approximate solutions for the time dependence of the birefringence, Δn, under low electric field conditions. The perturbation method of Matsumoto et al.[17] gives $\Delta n(t)$ for cases where the polarization relaxation time, τ_p, is much less than $1/(6D_r)$. In their treatment three time domains are considered which correspond to the sudden application of the electric field, the sudden reversal in polarity, and the sudden removal of the field. The equations that describe the birefringence of monodisperse cylindrical particles at low electric fields are

rise:

$$\Delta n(t) = \Delta n_0\left\{1 - \frac{3R}{2(R+1)}e^{-2D_rt} + \frac{R-2}{2(R+1)}e^{-6D_rt}\right\} \tag{16a}$$

reversal:

$$\Delta n(t) = \Delta n_0\left\{1 + \frac{3R}{R+1}(e^{-6D_rt} - e^{-2D_rt})\right\} \tag{16b}$$

decay:

$$\Delta n(t) = \Delta n_0 e^{-6D_rt} \tag{16c}$$

where Δn_0 is the steady-state amplitude of the birefringence for a particular electric field, R is the ratio of permanent to induced dipole terms ($R = \mu^2(\Delta\alpha kT)^{-1}$), and kT is the thermal energy.

Reversal of the electric field can also be used to determine the relaxation time, τ_p, of the ionic polarizability for cases where the polarization time is on the order of the rotational time, i.e., when $\tau_p \approx 1/(6D_r)$. Sudden reversal of the orienting field forces molecules with a permanent moment or a slow induced moment to reorient. The transient signal produced by the reorienting molecules permits one to distinguish the type of orientation mechanism and, for cases where slow polarization processes dominate, to determine its relaxation time. The treatment given by Tinoco and Yamaoka[18] can be used as a first approximation to describe the transient behavior observed upon sudden reversal of the orienting electric field.

In the birefringence experiment,[19] linearly polarized light enters an isotropic system of molecules and exits unchanged in polarization. However, when the molecules are ordered by an electric field pulse, the entering light becomes elliptically polarized because one component of the light is retarded. A quarter-wave plate converts the exiting elliptical light back to linear polarization rotated by $\delta/2$ from the original. The time response of δ corresponds to the time evolution of molecular ordering and it is related to the change in light intensity as discussed below.

The light intensity that passes through the analyzer as a result of an external electric orienting pulse is given by

$$I(t) = I_0K\{\sin^2(\beta - \alpha(t)/2) + K_{ex}\} \tag{17}$$

where I_0 is the intensity of the light incident on the sample, K is a light reflection and absorption loss factor ranging between 0 and 1, β is the angle between the analyzer and

its crossed position, and K_{ex} is the overall extinction ratio. The extinction ratio, $I(0)_{\beta=0}/I(0)_{\beta=\pi/2}$, is an indication of the quality of the optical components. The relative change in the intensity due to the birefringent nature of the ordered system is

$$\frac{\Delta I(t)}{I_\beta} = \frac{\sin^2 [\beta - (\pi l/\lambda_0)\Delta n(t)] - \sin^2 \beta}{\sin^2 \beta + K_{ex}} \quad (18)$$

where $\Delta n(t)$ is given by eq 16.

For those cases in which β is chosen to be less than 10° and much greater than $\delta_0/2$, where δ_0 is the steady-state retardation, eq 18 reduces to a simpler form, which is linear in $\Delta n(t)$. For example, the decay of the birefringence under these conditions is given by

$$\Delta I(t) = \Delta I(0)e^{-t/\tau_r} \quad (19)$$

Thus, by measuring the time dependence of the light intensity, one can obtain the relaxation time, $\tau_r = 1/(6D_r)$, directly.

Experimental Section

Samples. 1. Restriction Fragments. The restriction fragments used in this study were from two sources: the plasmids pBR322 and pMB9. The pBR322 plasmid has been completely sequenced,[20] but the genetically related pMB9 plasmid has not. However, many of the digestion products of pMB9 are the same as pBR322 and so for these fragments the number of base pairs is known. Of the thirteen restriction fragments used in this study there were three whose base pair number was not known exactly. Two of these (410 and 950 base pairs) were sized on analytical gels. The 410 base pair sample was actually an equal molar mixture of 405 and 415 base pair fragments. The exact size of the 5000 base pair fragment of pMB9, which was kindly provided by M. Fried, is not known but it is linear pMB9 prepared by digestion with *Eco*RI. The short restriction fragments used were from a *Hae*III digest of pBR322 and were kindly provided by M. Mandelkern. All other fragments were from a *Hae*III or *Eco*RI digest of pMB9. The procedure followed in preparing the pMB9 plasmid has been described elsewhere.[21] The only modification to this procedure was that uridine was added just before the addition of chloramphenicol to enhance plasmid production.[22]

Haemophilus aegyptius ATCC 1116, *Hae*III, restriction endonuclease (New England Biolabs) was used at a concentration of 0.2 unit/μg of DNA for 20 h at 37 °C to digest the plasmid. The digestion products were separated on a prerun 5% polyacrylamide slab gel. Sixteen digestion products were excised from the gel, using ethidium bromide and UV light to locate each band. The gel was exposed to UV light for a very brief time, just long enough to excise the bands. Each fragment was electrophoretically eluted into dialysis tubing which contained a small volume of Tris–borate–EDTA buffer.

After electrophoretic elution, the samples may contain free acrylamide, which constitutes an impurity. We found that the birefringence signal was dominated by a positive component unless the impurities were first removed by washing each fragment on a small DEAE-Bio-Gel-A column with 50–100 bed volumes. The DNA was eluted with a 4 M NaCl–Tris buffer and the remaining ethidium bromide was removed by several 2-propanol extractions. Ether was used to remove dissolved 2-propanol. The samples were extensively dialyzed at 4 °C against several changes of buffer to the final salt concentration. The buffer was sodium phosphate adjusted to a sodium ion concentration of 1.0 mM and pH 7.2. The sample concentrations were measured with a Cary 219 spectrophotometer and were the same (~5 μg of DNA/cm^3) for all the experiments.

Some important details should be considered when preparative polyacrylamide gel electrophoresis is used to prepare DNA for birefringence or dichroism studies. We found that it was absolutely necessary to prerun the acrylamide gel for several hours before loading the DNA onto it. If the gel is not prerun, the DNA will associate with one of the polymerizing ions and its electrical properties will be altered drastically. Specifically, the DNA acquires an asymmetric charge that results in a large permanent dipole moment. This additional moment is easily detected in a birefringence experiment using a reversing electric field pulse, as we have done, by observing the transient behavior of the light intensity. The measured R value ($R = \mu^2/\Delta\alpha kT$) for nonprerun gel prepared samples was approximately 1.5, where normally the transient dip for DNA results in a calculated R value of less than 0.1. This is an enormous increase in the permanent dipole moment of DNA and is equivalent to a permanent moment greater than 8000 D. This phenomenon would also be detected by comparing the rise time to the decay time calculated from single exponential fits. Equation 16 shows that the rise time for molecules possessing a permanent dipole moment is longer than the decay time. For R values this large, the rise time would be approximately twice the decay time. The birefringence signal for the rise, the field reversal, and the decay fitted well the theoretical curve, eq 16, for a molecule having a permanent dipole moment of this magnitude. This provides further evidence that the DNA acquired an additional permanent moment. In order to avoid these problems we preran the gels for the time it took Xylene Cyanol FF to migrate to the bottom of the gel.

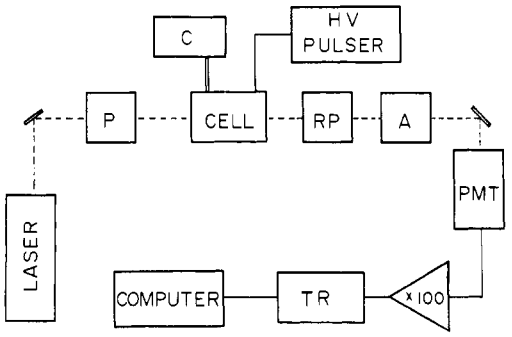

Figure 1. Schematic diagram of birefringence apparatus. Laser, argon, Lexel Model 95; C, Lauda bath and circulator; P and A, Glan-Thompson polarizers; cell, birefringence sample cell and thermostatic container; HV pulser, Cober Model 605P and Velonex Model 350 high-voltage pulse generators; RP, quarter-wave plate; PMT, 1P28 phototube; X100, Textronix Model 1121 amplifier; TR, LeCroy 2256 transient recorder; computer, LSI-11 computer.

2. Nucleosomal DNA. The 145 base pair DNA was prepared by mild micrococcal nuclease digestion of chicken blood chromatin followed by sucrose density gradient fractionation to isolate a narrow band of monomers. This was followed by protease digestion of the nucleosome monomers and phenol extraction to remove proteins. The procedure is essentially that described by Simpson[23] and modified slightly by Mandelkern.

The resulting samples were shown by gel electrophoresis to be fairly monodisperse and span a distribution of approximately 20 base pairs centered at 145 base pairs. In birefringence tests on these samples the decay times were all single exponential and the relaxation times did not change with field strength over the range 0–7 kV/cm. Therefore, the usual criteria for monodispersity were satisfied.

All of the samples were extensively dialyzed at 4 °C against the appropriate buffer at pH 6.5. For the Na^+ dependence experiments a phosphate buffer was used and for the Mg^{2+} experiments we used a magnesium acetate buffer. The samples used for the lowest salt concentrations were ethanol precipitated with the appropriate counterion and then dissolved in doubly deionized water, which was used for all of the sample preparations.

Apparatus. The birefringence apparatus used for this work was designed to measure moderately fast and relatively weak birefringence signals. Use of laser illumination combined with fast analog-to-digital conversion and signal averaging resulted in a birefringence amplitude sensitivity of 4×10^{-12} and time resolution of 50 ns. The orientating electric field can be used as an alternating unipolar pulse or as a reversing bipolar pulse, and its amplitude is variable up to 7.5 kV/cm with fast rise and decay times. The apparatus is similar in many respects to previously reported designs,[24] but it has several significant differences. A block diagram is given in Figure 1 and a brief description follows.

The light source is a Lexel Model 95 argon ion laser operating at 514.5 nm. The laser beam passes first through a high-quality

Glan-Thompson polarizer and then is reduced to 1 mm in diameter with a pinhole before it enters the sample cell. The cell was machined from a solid block of polycarbonate and has an optical path length of 30 mm and electrode gap of 2.7 mm. The sample volume is 0.7 cm^3. The cell windows are 8.1-mm-thick optical glass and are attached, with minimal strain, to the cell body with cover plates. Strain birefringence is negligible. A calibrated thermistor is embedded in the cell body adjacent to the sample. The cell is completely encased by a thermostated aluminum block which has 6-mm-diameter optical entrance and exit holes. The temperature is constantly monitored during an experiment and is controlled to ±0.02 °C. A mica quarter-wave plate is placed directly behind the cell compartment. Following the quarter-wave plate is a Glan-Thompson analyzer, whose angular position is adjustable to ±.001°, and a 1P28 phototube. The extinction ratio, K_{ex}, for the complete system, including the cell, is 1×10^{-6}. Directly before the phototube, which is encased in a light-tight container, is an interference filter and diverging lens. The filter passes only laser light and the lens spreads the beam onto the photocathode. The phototube is terminated with 200 Ω to give fast response (<50 ns). The resulting voltage is amplified by an ac-coupled Tektronix 1121 amplifier and digitized by a LeCroy 2256 transient recorder having 8-bit resolution and a maximum digitizing rate of 20 megasamples per second. Each birefringence signal is stored in 1024 words of digitizer memory and later transferred, between high-voltage pulses, to an on-line DEC LSI-11 computer via a lab-designed interface. The computer stores the birefringence signals and after the requested number of accumulations it calculates the amplitude, fits the rise, reversal, or decay portions of the curve, using eq 16 and 18, plots the raw data, and stores the data on disk. During the experiment, the accumulated birefringence signal is displayed on a large-screen oscilloscope so that the buildup of the signal can be followed.

The high-voltage exciting pulse is produced by coupling, in parallel, Cober Model 605P and Velonex Model 350 high-power pulse generators. The Velonex produces the negative pulse and the Cober the positive pulse. When a unipolar exciting pulse is desired, the Cober generator is used, and the pulse polarity is alternated with mercury-wetted switches to prevent electrode polarization. The pulse length is continuously adjustable from several hundred nanoseconds to 10 ms. The electric field is continuously variable from 0 to 7.5 kV/cm, and it is accurately measured for each run by a high-voltage pulse amplitude meter. The high-voltage switching time is approximately 100 ns, which is much faster than the relaxation times of all but the smallest restriction fragments.

The procedure used to accumulate a birefringence signal is as follows. The sample is degassed in the cell and its conductance is measured and recorded. The angle β between the analyzer and its fully extinguished position, crossed with the polarizer, is chosen to achieve optimal signal to noise. Once β is chosen and the laser power adjusted to an appropriate level, the background intensity, I_0, is measured by chopping the laser beam. The photomultiplier tube output of the chopped beam is amplified, digitized, and averaged, using the same electrical components as in the birefringence determination. This permits a direct comparison between the background intensity and the signal of interest. The birefringence signal, $\Delta I(t)$, is then averaged and its steady-state amplitude is automatically calculated by the computer using

$$\Delta n_0 = (\lambda_0/\pi l)\{\beta - \arcsin [(\Delta I_0/I_0)(\sin^2 \beta + K_{ex}) + \sin^2 \beta]^{1/2}\} \quad (20)$$

where $\Delta I_0/I_0$ is the relative amplitude of the laser light corresponding to the steady-state birefringence. Since our usual sample concentration is very low, the contribution of water birefringence, Δn_w, to the total signal, Δn_0, is significant and is therefore subtracted. All of the experiments were done at 4 °C and at electric fields below 2.5 kV/cm.

As a check of the system's capability we measured the birefringence of water at low electric fields. The Kerr law was obeyed at all field values, as it should be for water, and resulted in a Kerr constant of 3.44×10^{-12} cm/V^2 at room temperature. The sensitivity of the system is demonstrated by the fact that the birefringence of water can be measured at fields as low as 150 V/cm, which is equivalent to a birefringence of 4×10^{-12}.

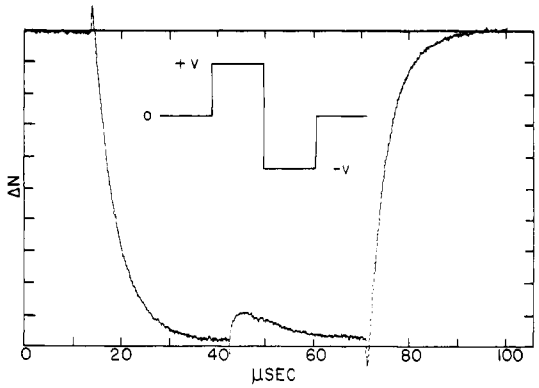

Figure 2. Typical example of a reversing low-field electric birefringence signal. The maximum in the center occurs when the applied electric field is suddenly reversed in polarity and the DNA molecules partially reorient. The spikes on the rising, reversal, and falling edges are due to the birefringence of water. Inset: Time-compressed waveform of the electric field.

Results

Figure 2 shows a typical birefringence signal for short fragments of DNA obtained with a reversing pulse electric field. The rise, reversal, and fall portions of the birefringence curve would be accurately described by eq 16 if the DNA possessed a permanent dipole moment. The time dependence of the transient which may occur upon field reversal is indicative of the orientation mechanism. For macromolecules that have a permanent moment the transient's extremum is completely determined by its rotational diffusion constant. In the case of slow polarization processes the transient's extremum depends on the relaxation time of the ionic species near the polyelectrolyte. In both cases, a transient in the birefringence will be observed upon field reversal, and the size and shape of it are determined by the orientation mechanism. The dependence of the transient as a function of ionic species and field strength will be reported in a later paper. For now, we can report that the transient maximum of the short fragments (<267 base pairs) occurs at a time shorter than that expected for macromolecules having a permanent dipole moment. Fragments between 267 and 5000 base pairs show an unusual transient behavior upon field reversal: an additional component of opposite sign occurs after the maximum which resembles closely that which would be expected for molecules having a transverse moment. The magnitude of the effect depends on both the contour length and the ionic strength and thus is related to the flexibility of the DNA.

All of the analyses described in this paper have used the field-free decay times and amplitudes obtained from low electric field experiments where the Kerr law was obeyed. The rotational relaxation times were all obtained from least-squares fits of the decay portion of the birefringence curves. We found that for fragments above 400 base pairs each decay curve was a sum of two exponentials, one long and one very short with a small amplitude. For these fragments the longer times were used in the hydrodynamic analysis. The Kerr constants were all obtained from linear least-squares fits of Δn vs. E^2. All of the experiments were done in the Kerr law region and we limited the electric field to 2.5 kV/cm for even the small fragments. The birefringence rise times were always found to be longer than the decay times which is expected for molecules showing a transient upon field reversal. The results of the experiments on the restriction fragments are presented in Table I and those in the 145 base pair nucleosomal fragments in Table II.

Table I
Birefringence Properties of DNA Fragments Measured at 4 °C in 1 mM Na^+

no. base pair	DNA concn, g/cm³	$10^6\tau_r$, s	$10^{-3}D_r^{20}$, s^{-1}	L_{eff}, Å	$10^{15}\Delta\alpha$, cm³
64	5.2	0.48	587	200	0.036
80	5.6	0.80	332	252	0.058
89	5.0	1.18	253	296	0.104
104	5.2	1.67	172	340	0.165
124[a]	5.2	2.25	126	381	0.229
145	7.2	3.67	75.1	469	0.307
188[b]	5.1	5.76	49.0	561	0.413
213	5.9	8.38	34.1	639	0.522
234	4.6	9.22	30.4	670	0.609
267	4.6	11.94	23.8	741	0.676
410[c,d]	5.1	34.5	7.99	1113	1.36
587	5.0	71.0	3.88	1463	1.47
950[d]	6.3	174.0	1.58	2046	3.46
5000	4.9				21.6

[a] Equal molar fractions of 123 and 124 base pair fragments. [b] Equal molar fractions of 184 and 192 base pair fragments. [c] Equal molar fractions of 405 and 415 base pair fragments. [d] Size determined from analytical gels.

Rotational Diffusion Constant. Length Dependence. Figure 3 is a log-log plot of the measured relaxation times vs. the number of base pairs cubed shown along with the theoretical curves predicted by rigid rod, weakly bending rod, and wormlike coil models. The solid line corresponds to the rigid rod model and was calculated from eq 1, using 3.15 Å as the rise per base pair, a diameter of 27 Å, and Broersma's γ_r function, eq 2. We use 3.15 Å as the rise per base pair because it is consistent with recent quasi-elastic light scattering results.[25] The graph clearly indicates that DNA at this concentration and ionic strength does not behave strictly like a rigid rod beyond approximately 120 base pairs. This assertion also holds true for the Yoshizaki and Yamakawa form of eq 1. The first four points agree very well with their theory when we use 53 Å for the diameter and 3.15 Å for the rise per base pair. The agreement is not quite as good if we use a diameter of 34 Å and 3.4 Å for the rise per base pair or if we limit the diameter to 26 Å and use 3.5 Å. This coupled variation of the parameters RPB and d holds for all forms of eq 1 and therefore we have used the equations only to indicate the point at which DNA begins to depart from a rigid straight cylindrical rod. In order to determine the rise per base pair unambiguously, one must remove the dependence upon the diameter. This was done by combining our rotational diffusion measurements with translational diffusion measurements from a quasi-elastic light scattering experiment.[25]

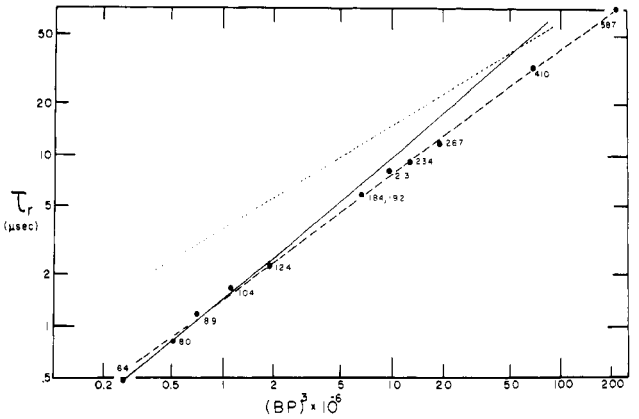

Figure 3. log-log plot of the rotational relaxation times vs. the number of DNA base pairs cubed. The circles represent the experimental points. The solid line was calculated from Broersma's equation (eq 1 and 2), using 3.15 Å for the rise per base pair and 27 Å for the diameter. The dashed line was calculated from Hearst's weakly bending rod model (eq 5), using 495 Å for the persistence length, 3.15 Å for the rise per base pair, 30.4 Å for the distance between frictional elements, and 27 Å for the diameter. The dotted line was calculated from Hearst's wormlike model (eq 4), using the same parameters as above. All of the experiments were done at 4 °C and in 1 mM Na^+.

As Hearst[7] has suggested, eq 4 for the rotational diffusion constant of a wormlike coil can be rearranged to a form which permits the graphical determination of Q, the persistence length, independent of the values of a and b. However, our graphic analysis gives an unphysical result: a negative persistence length.

Unlike the case of the wormlike model, there is no simple graphical method to obtain the persistence length using the weakly bending rod model, eq 5, which is independent of the parameters a and b. However, if one is interested in just the persistence length and not the Stokes diameter, a, or the length per frictional element, b, then eq 5 can be used in a slightly different form which allows the persistence length to be determined accurately. Replacing the rotational diffusion constant with $1/(6\tau_r)$ and rearranging terms in eq 5 gives

$$Y(\mathrm{BP},a,b,\mathrm{RPB},\tau_r) = \frac{1}{Q}X(\mathrm{BP},a,b,\mathrm{RPB}) \qquad (21)$$

where Y and X are given by

$$Y = \frac{L^3}{\tau_r} - \frac{6kT}{\eta_0\pi}\left(3\ln\frac{L}{b} - 7.0 + 4\left(\frac{b}{a}\right)\right) \qquad (22)$$

$$X = \frac{6kT}{\eta_0\pi}\left\{\frac{L}{2}\left(2.25\ln\frac{L}{b} - 6.66 + 2\left(\frac{b}{a}\right)\right)\right\} \qquad (23)$$

Table II
Birefringence Properties of 145 Base Pair Nucleosomal DNA Measured at 4 °C in the Presence of Different Counterions

DNA concn, μg/cm³	counterion	ionic strength × 10^3	$10^6\tau_r$, s	$10^{-4}D_r^{20}$, s^{-1}	L_{eff}, Å	$10^{15}\Delta\alpha$, cm³
3.5	Na^+	0.012	4.11	6.71	488	0.421
6.5	Na^+	0.6	3.84	7.18	475	0.381
7.2	Na^+	1.2	3.67	7.51	466	0.307
7.0	Na^+	2.4	3.72	7.41	469	0.236
8.25	Na^+	4.8	3.30	8.35	447	0.152
8.5	Na^+	7.7	3.14	8.78	438	0.113
6.75	Na^+	12.2	3.18	8.67	440	0.069
6.25	Mg^{2+}	0.03	3.34	8.25	449	0.279
6.1	Mg^{2+}	0.55	3.25	8.48	444	0.199
6.0	Mg^{2+}	1.25	3.29	8.38	446	0.154
6.5	Mg^{2+}	2.5	3.24	8.51	443	0.106
5.5	Mg^{2+}	5	3.32	8.30	448	0.075

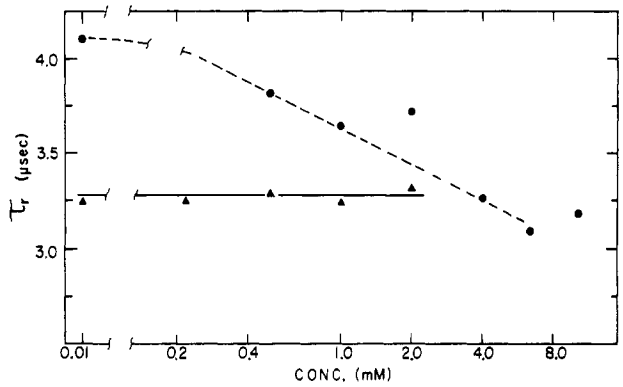

Figure 4. Rotational relaxation times of the 145 base pair DNA vs. the log of the counterion concentration. The circles represent the NaDNA data and the triangles represent the MgDNA data.

where the contour length L = (BP − 1)(RPB) + $C \approx$ (BP)(RPB) with C equal to a small constant.

A linear least-squares fit of Y vs. X for samples and their corresponding τ_r's gives the persistence length, Q, from the slope. The persistence length and its uncertainty determined from the fit depend on the initial estimate for the parameters a, b, and RPB. By doing iterative fitting to eq 21 with a, b, and RPB as free parameters, we can obtain the correct persistence length. These assertions were tested by simulations. Starting with arbitrary values of a, b, and RPB, the iterative fit always determined Q within 1% while the values of a, b, and RPB differed considerably from their actual values. If, however, reasonable limits are placed on the Stokes diameter, say 20 Å $\leq a \leq$ 30 Å when the actual value of a is 25 Å, then RPB is also determined quite accurately, but with a and b still in considerable error.

The dashed line in Figure 3 was calculated from the weakly bending rod model, using eq 5 with 3.15 Å as the rise per base pair, 27 Å for the Stokes diameter, 30.4 Å for the frictional element spacing, and 495 Å for the persistence length. These parameters were obtained by using an iterative fit to eq 21 as described above in which we limited the Stokes diameter to a maximum of 27 Å and the rise per base pair to a minimum of 3.15 Å to be consistent with our other results.[25] The fit is very sensitive to both the persistence length and the rise per base pair but not to the Stokes diameter and frictional element spacing.

To demonstrate the lack of agreement between our results and the wormlike coil model we have plotted the theoretical predictions for the rotational diffusion constant in Figure 3 as the dotted line, using the same parameters as used for the weakly bending rod model. Note that although there is no agreement, the results for the wormlike coil approach our data for large DNA fragments.

Rotational Diffusion Constant. Counterion Dependence. Figure 4 shows the dependence of the field-free decay time for chicken blood DNA with either Na^+ or Mg^{2+} as the counterion. The decay time decreases with increasing Na^+ concentration up to 4 mM Na^+, but it is invariant to changes in Mg^{2+} concentration over the entire range studied. The total change in the relaxation time corresponds to an effective length increase greater than 10%. This phenomenon was also observed for the 184,192 base pair restriction fragments with Na^+ as the counterion and so it appears that it is not a result of the small polydispersity in the nucleosomal DNA.

Polarizability. Length Dependence. The polarizability as a function of DNA length is shown in Figure 5 along with the theoretical predictions of Fixman, eq 14, and Mandel, eq 9, which has been scaled to equal the point

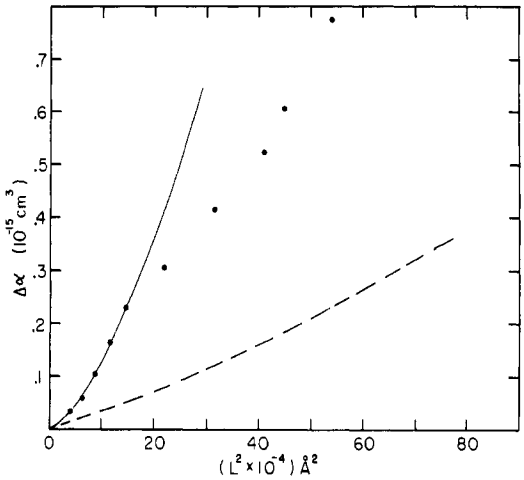

Figure 5. Polarizability vs. the hydrodynamic length squared. The circles represent the experimental points. The dashed line was calculated from Fixman's theory and the solid line was calculated from the Mandel theory scaled to the point at 124 base pairs.

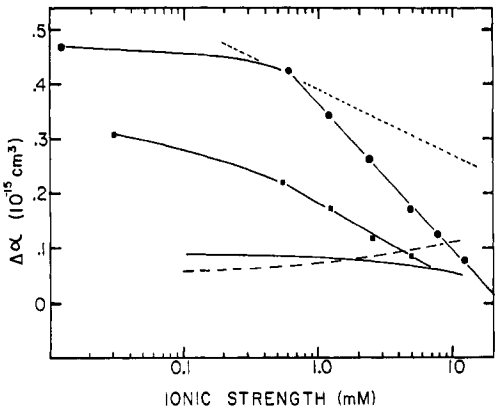

Figure 6. Polarizability of 145 base pair DNA vs. the log of the ionic strength. The circles represent the NaDNA experimental values and the squares represent the MgDNA experimental values. The theoretical curves were calculated for Na^+. The dashed line was calculated from Manning's theory (eq 9), the solid line was calculated from Fixman's theory (eq 14), and the dotted line from Oosawa's theory (eq 8), using an adjustable parameter to match his theory with experiment near 1 mM.

at 124 base pairs. The polarizabilities were calculated from the measured Kerr constants using

$$\Delta\alpha = \frac{n_0^2 15kT}{(1 + R)2\pi\Delta g} K_{sp} \tag{24}$$

where n_0 is the refractive index of the solvent (n_0 = 1.33), R (see eq 16) is taken to be zero in these calculations, Δg is the optical anisotropy factor equal to −0.0215,[2] and K_{sp} is the specific Kerr constant given by

$$K_{sp} = \frac{1}{c_v n_0} \lim_{E \to 0} \frac{\Delta n_{DNA}}{E^2} \tag{25}$$

where c_v is the volume fraction of the DNA calculated using 0.50 cm^3/g for the partial specific volume.[26] For the concentration determination we used 1.0 OD_{260} = 50 μg of DNA/cm^3. The Kerr constants, $\lim_{E \to 0} (\Delta n_0/E^2)$, were obtained from the least-squares fits of the birefringence values vs. electric field squared. The abscissa of Figure 5 represents the hydrodynamic length squared, where the hydrodynamic length for each restriction fragment was calculated by using eq 1 and 2. Therefore, this length

represents an effective length and not the contour length.

Polarizability of Nucleosomal DNA. Counterion Dependence. Figure 6 shows the polarizability values obtained for the 145 base pair nucleosomal DNA as a function of the logarithm of the ionic strength. Two significant points should be noted concerning the results in Figure 6: (1) the polarizability is a decreasing linear function of the log of the ionic strength over a wide range of counterion concentration and (2) the polarizability of DNA with Na^+ as counterion is larger than it is with Mg^{2+} as the counterion, in contrast to a previous result.[10]

Discussion

Our hydrodynamic results can be summarized as follows. The hydrodynamic behavior of DNA over a wide range of lengths in 1 mM Na^+ solution can be described reasonably by the weakly bending rod model but not by the wormlike model. The fact that the wormlike model fails to fit the experimental results is not surprising since most of our data are for low molecular weight DNA (<600 base pairs) with a resulting small number of frictional elements. The prediction for the rotational diffusion constant within the framework of the weakly bending rod model is expected to hold in the limit that the contour length is much less than 4 times the persistence length. Although this condition is not satisfied for many of our samples, we find that we can apply the theory to samples with a contour length equal to 4 times the persistence length.

The persistence length at 1 mM Na^+ salt concentration was found to be 500 Å. This conclusion, however, depends explicitly on the weakly bending rod model of Hearst. Our persistence length agrees well with Kovacic and van Holde's[3] sedimentation velocity result of 575 Å, where they used a diameter of 27 Å. However, it is not appropriate to make a direct comparison with their results since our experiments were done at a lower ionic strength, where the persistence length is expected to be greater. Other investigations, although none based upon rotational diffusion measurements, indicate that the persistence length is much larger than 500 Å under the low salt conditions of our experiment. Therefore, we must question whether the persistence length as determined from Hearst's weakly bending rod model is the same quantity as that determined in other experiments.

The field-free decay time is shown in Figure 4 to decrease with Na^+ concentration over a certain salt range. However, it does not vary when Mg^{2+} is the counterion. We attribute this behavior to an effective length change of the 145 base pair DNA due to electrostatic repulsions along the DNA backbone.

With Na^+ as the counterion the effective screening of the phosphate charges is less than it is when Mg^{2+} is the counterion. Below 4 mM, repulsions between neighboring phosphates increase because fewer Na^+ counterions are available for shielding. Hence, there is a subsequent stretching or stiffening of the chain and a resulting increase in the rotational diffusion time. Our persistence length measurements indicate that it is quite possible that we are observing chain stiffening rather than an increase in contour length. A detailed study of the ionic strength dependent phenomena for the restriction fragments is now under way in this laboratory.

There are other possible explanations of this behavior. The DNA helix may be unraveling slightly as the ionic strength is reduced. This would account for the increased relaxation time, assuming that the friction coefficient increased with unraveling. It is, however, unlikely that unraveling of the helix is the cause of the increased relaxation time since T_m is greater than 50 °C and all of the experiments were done at 4 °C. Even if T_m is lower, it is unclear whether the small change in the Na^+ concentration could cause sufficient melting to produce the observed effects. It is also possible that we are observing a change in the rotational relaxation time due to a coupled ion effect which becomes significant at Na^+ concentrations below 4 mM. We shall explore this possibility more fully in the future.

The hydrodynamic behavior of DNA in 1 mM Na^+ is not strictly rigid rodlike beyond approximately 120 base pairs. This result seems to be supported by the observations that the relaxation time data begin to fall away from the theoretical curve for rigid cylinders beyond 124 base pairs and that the relaxation time increases with decreasing Na^+ concentration, which may indicate chain stiffening. As discussed below, the polarizability also departs from a cubic length dependence beyond 124 base pairs.

The counterion concentration dependence of the polarizability can be described qualitatively as follows. The electrical polarizability of polyelectrolytes is a measure of the relative ease with which charges of opposite sign separate in a perturbing electric field and give rise to an electric dipole moment. In the simplest analysis we can image that under equilibrium conditions the counterions are localized near the permanently charged sites along the DNA backbone. When an external electric field is introduced, the mobile counterions migrate away from their equilibrium positions and settle into a steady-state configuration, which is determined by the local electrostatic fields. These local fields are in part due to repulsive interactions between neighboring counterions. Thus, when counterion local densities increase, both shielding of the external field and counterion–counterion repulsive forces increase, and there is a smaller charge displacement and subsequently lower induced dipole moment.

The polarizability shown in Figure 6 is larger when Na^+ is the counterion than it is when Mg^{2+} is the counterion. In the case of Mg^{2+} the counterion–counterion repulsive forces are longer ranged than they are for Na^+. Therefore, for a particular electric field the polarization and thus the net orientation will be less than it is at the same Na^+ concentration. In simpler terms, the Mg^{2+} counterions still greatly influence their neighboring counterions even under the condition of zero added salt. In addition to the larger repulsive force between divalent counterions, there is a larger attractive force between the divalent counterions and the backbone charge than there is between the univalent counterion and the backbone charge. This reduces the net polarization of the divalent counterion compared to that of the univalent counterion and leads to less net orientation and a smaller Kerr constant.

Another point concerning Figure 6 is that the two experimental slopes for Na^+ and Mg^{2+} are not the same, in contrast to the data shown in Figure 6 of ref 1. If we refer to Figure 4 in this paper, we see that the effective length of the DNA changed with Na^+ concentration but not with Mg^{2+}. Therefore, the NaDNA polarizability is expected to show a steeper slope than the MgDNA does because, as the Na^+ salt concentration is lowered, the DNA length increases. An increase in the polarizability with decreasing Na^+ salt results not only because there is less counterion–counterion repulsion but also because there is a length increase of the DNA. If we assume that the functional dependence of the polarizability is cubic and then correct the data to take into account the length change, we get nearly the same slope with both Na^+ and Mg^{2+} as counterions.

Also shown in Figure 6 are the theoretical predictions of Fixman, Manning, and Oosawa. The Oosawa curve was

calculated from eq 8 by using w/c in place of the counterion phase radius parameter a, where c is the molar concentration of the counterion, and where w was chosen so that the calculated polarizability matched the experimental value near 1 mM. The parameter R_v was calculated to be 2000 Å, the rise per base, RPB, was 3.15 Å, and γ was 0.78. The functional dependence, as pointed out by Hornick and Weill,[10] is then consistent with experiment, with the exception that the theoretical slope is less than the actual slope.

It would seem that the Oosawa theory, eq 8, correctly accounts for the polarizability counterion dependence. We must point out, however, that eq 8 was derived from eq 7 under the constraint that $L \gg d$ and therefore the cylindrical free volume model may not be appropriate. In any event, eq 8 cannot be directly applied to experiment since the concentration dependence of the counterion phase radius is not known.

The Manning theory, eq 9, shows an increasing polarizability with added salt. This trend could be reversed if the charge fraction parameter were allowed to decrease with increasing salt concentration. In order for the theory to match the experimental slope, the charge fraction would have to decrease by 25% over the concentration range studied. However, even a small change in the charge fraction would violate the rules of the condensation theory.[27] Warashina and Minakata's[11] theory also shows that the polarizability increases with increasing counterion concentration.

It seems, then, that only Fixman's theory, eq 14, explicitly shows the correct trend in the polarizability as a function of counterion concentration. In his treatment of the polarizability he indicates that the integral equation which describes the electrostatic potential is modified by the passage of counterions through the double layer surrounding the DNA. This flux acts to reduce the induced moment. The approach used in his treatment is strictly valid only if the DNA's radius of curvature is greater than the Debye length and therefore at low salt concentrations the flux may be overestimated. This may explain the discrepancy between our results and his predictions.

Figures 5 and 6 show that the polarizability of NaDNA is considerably greater than that predicted for rigid rods by the Mandel–Manning and Fixman theories for counterion concentrations near 1 mM. In spite of the discrepancy between theory and experiment for the magnitude of the polarization, it is of interest to consider the predicted length dependences. In the limit of small ρ Fixman's theory has roughly a cubic length dependence. This limit occurs when the equilibrium number of counterions per unit length ϵ is large, as in the case of a conducting cylinder in a parallel field, or when the counterion concentration and length are small. For DNA in 1 mM Na^+ this cubic length dependence is predicted to hold for lengths much shorter than our shortest fragment. The Mandel–Manning theory, eq 9, has a cubic length dependence for all lengths. The values predicted by this theory are smaller than Fixman's predictions up to a length of 500 Å and then become larger as the length increases (40% greater for a length of 900 Å).

One could achieve a reasonable fit to a quadratic length dependence over the entire range of fragments shown in Figure 5, in qualitative agreement with Fixman's predictions. However, if the polarizability had been plotted vs. the contour length squared instead of the hydrodynamic length squared, the experimental polarizability would be observed to vary more weakly than the square of the contour length for fragments larger than 145 base pairs.

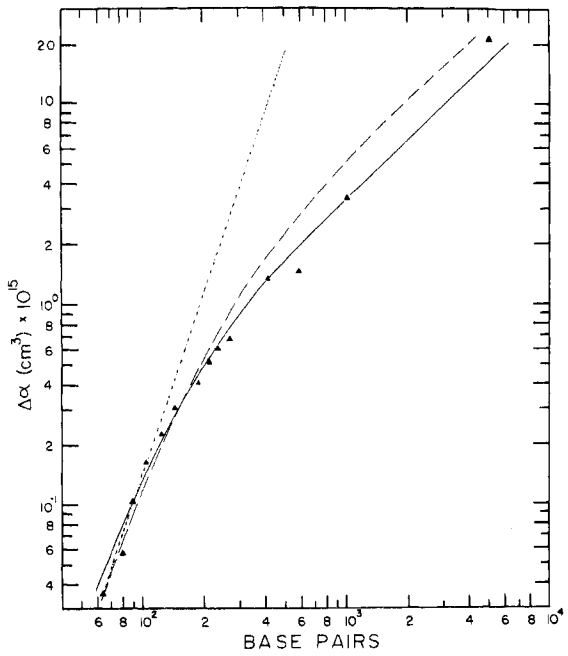

Figure 7. log–log plot of polarizability vs. the number of DNA base pairs. The triangles represent the experimental values which begin at 64 base pairs and end at 5000 base pairs. The solid and dashed curves represent our modification to Mandel's polarization theory calculated by using 320 and 500 Å, respectively, for the persistence length. The dotted line represents the cubic length dependence of the unmodified Mandel theory (eq 6).

In Figure 5 the solid line has been drawn with a cubic length dependence as predicted by Mandel's[8] theory so that it matches the experimental point at 124 base pairs. It can be seen that the five shortest fragments have polarizabilities which vary cubically with length and that the polarizabilities of the larger fragments fall off from a cubic dependence.

This result is exactly what one would expect if the polarizability length dependence is cubic and after 124 base pairs the DNA begins to deviate from rigid rod behavior. This interpretation is consistent with our rotational diffusion measurements that indicate that DNA is not strictly rodlike beyond 124 base pairs under these salt conditions.

In order to show the length dependence of the polarizabilities for all of our fragments, we have constructed a log–log plot of polarizability vs. number of base pairs in Figure 7. From 64 to 124 base pairs the polarizability is a cubic function of the number of base pairs but above 124 base pairs the dependence is weaker and approaches a value of 1.1 for sizes greater than 267 base pairs.

The flexibility of DNA will affect its optical anisotropy as well as the polarizability. Arpin et al.[28] have calculated the optical anisotropy of a wormlike chain and have applied the results to the determination of the persistence length of an aromatic polyamide using depolarized light scattering. van der Touw and Mandel[29] have determined the counterion polarization of a polyelectrolyte composed of a sequence of rodlike subunits in an arbitrary configuration and have used the prediction in the interpretation of dielectric increment and dispersion measurements. A proper treatment of the effect of flexibility of a polyelectrolyte on the measured Kerr constant requires an average calculated over both the optical and counterion polarization terms. We expect that this calculation will lead to a result in which for short, stiff molecules the Kerr constant (and the counterion polarization) will be cubic in the contour length and that for long, flexible molecules the Kerr constant will be linear with the contour length.

In our analysis we have taken the optical anisotropy to be a constant independent of length[2] and therefore the specific Kerr constant will scale with the polarizability, $\Delta\alpha$. Mandel's[8] expression for $\Delta\alpha$, eq 6, was derived for rigid cylinders and therefore does not account for any flexibility of the macromolecules. If we assume that the net induced dipole moment is a summation of individual dipoles along the DNA backbone, then any bending of the DNA will reduce the polarizability because of a loss of correlation between individual dipoles. For rigid rods the total projection is proportional to the number of charged sites or equivalently to the rod length. In the case of flexible rods, the projection is the vector sum of the individual dipoles along one direction and is therefore proportional to the contour length for short molecules and equal to the persistence length for long molecules. We have modified eq 6, which was derived for right circular cylinders, by replacing the contour length, L, with the average projection along the DNA's major axis. The modified equation is

$$\Delta\alpha = \frac{\gamma z e_0^2 N \langle Z_p \rangle^2}{12kT} \pi(c) \tag{26}$$

where the projection for a wormlike coil is

$$\langle Z_p \rangle = Q(1 - e^{-(\mathrm{RPB})(\mathrm{BP})/Q}) \tag{27}$$

and where Q is the persistence length, BP is the number of base pairs, RPB is the rise per base pair, and $\pi(c)$ accounts for the counterion interactions. The dashed curve in Figure 7 has been calculated by using eq 26 with γ = 0.78, a rise per base pair of 3.15 Å, and a persistence length of 500 Å, with $\pi(c)$ adjusted to a value of 2.3 to give the best agreement with experiment. The solid line was obtained by fitting the data to eq 26 with Q and $\pi(c)$ as free parameters. The resulting value of the persistence length is 320 Å and $\pi(c)$ is 4.1.

The modified Mandel equation is consistent with the experimental data: the polarizability starts out depending on the cube of the contour length, passes through a quadratic region, and then goes to a linear dependence in the limit of long molecules. The agreement between our modification to the theory and experiment is better with the lower value of the persistence length but we do not attach any special significance to this value. The important point is that the functional dependence is consistent with experimental results in spite of the approximations in our modification.

Acknowledgment. We are indebted to M. Fried for demonstrating the restriction fragment preparation and for providing the 5000 base pair fragment and to M. Mandelkern for demonstrating the nucleosomal preparation and providing the pBR322 fragments. We thank E. Charney, D. M. Crothers, N. Dattagupta, and T. Keyes for useful discussions. This work has been supported in part by Grant S07-RR-07015 from NIHBRS and Grant CHE 78-02922 from NSF.

References and Notes

(1) Hogan, M.; Dattagupta, N.; Crothers, D. M. *Proc. Natl. Acad. Sci. U.S.A.* **1978**, *75*, 195.
(2) Sokerov, S.; Weill, G. *Biophys. Chem.* **1979**, *10*, 161.
(3) Kovacic, R. T.; van Holde, K. E. *Biochemistry* **1977**, *16*, 1490.
(4) Perrin, F. *J. Phys. Radium* **1934**, *5*, 497. Burgers, J. M. *Verh. K. Ned. Akad. Wet.* **1938**, *16*, 113.
(5) Broersma, S. *J. Chem. Phys.* **1960**, *32*, 1626.
(6) Yoshizaki, T.; Yamakawa, H. *J. Chem. Phys.* **1980**, *72*, 57.
(7) Hearst, J. E. *J. Chem. Phys.* **1963**, *38*, 1062.
(8) Mandel, M. *Mol. Phys.* **1961**, *4*, 489.
(9) Oosawa, F. *Biopolymers* **1970**, *9*, 677.
(10) Hornick, C.; Weill, G. *Biopolymers* **1971**, *10*, 2345.
(11) Warashina, A.; Minakata, A. *J. Chem. Phys.* **1973**, *58*, 4743.
(12) Manning, G. S. *Biophys. Chem.* **1978**, *9*, 65.
(13) (a) Fixman, M. *J. Chem. Phys.* **1980**, *72*, 5177. (b) *Macromolecules* **1980**, *13*, 711.
(14) Riseman, J.; Kirkwood, J. G. "Rheology"; Academic Press: New York, 1956; Vol. 1, 495.
(15) Hermans, J. J.; Ullman, R. *Physica* **1952**, *18*, 951.
(16) McTague, J. P.; Gibbs, J. H. *J. Chem. Phys.* **1966**, *44*, 4295.
(17) Matsumoto, M.; Watanabe, H.; Yoshioka, K. *J. Phys. Chem.* **1970**, *74*, 2182.
(18) Tinoco, I.; Yamaoka, K. *J. Phys. Chem.* **1959**, *63*, 423.
(19) Fredericq, E.; Houssier, C. "Electric Dichroism and Electric Birefringence"; Oxford University Press: London, 1973.
(20) Sutcliffe, J. G. *Nucleic Acids Res.* **1978**, *5*, 2721.
(21) Bolivar, F.; Rodriquez, R. L.; Betlach, M. C.; Boyer, H. W. *Gene* **1977**, *2*, 75.
(22) Norgard, M. V.; Emigholz, K.; Monahan, J. J. *J. Bacteriol.* **1979**, *138*, 270.
(23) Simpson, R. T. *Biochemistry* **1978**, *17*, 5525.
(24) Newman, J.; Swinney, H. L. *Biopolymers* **1976**, *15*, 301.
(25) Mandelkern, M.; Elias, J. G.; Eden, D.; Crothers, D. M., submitted to *J. Mol. Biol.*
(26) Cohen, G.; Eisenberg, H. *Biopolymers* **1968**, *6*, 1077.
(27) Manning, G. *Q. Rev. Biophys.* **1978**, *11*, 1179.
(28) Arpin, M.; Strazielle, G.; Weill, G.; Benoit, H. *Polymer* **1977**, *18*, 262.
(29) van der Touw, F.; Mandel, M. *Biophys. Chem.* **1974**, *2*, 218.